Synthesis and Electrochemical Properties of ACNF/Li_2MnSiO_4 for Energy Storage Devices

Sukanya Nilmoung [a, *], Phanawan Whangdee [a], Pornpis Kongputhon [a],
Santi Maensiri [b, c]

[a] *Department of Applied Physics, Faculty of Sciences and Liberal Arts, Rajamangala University of Technology Isan, Nakhon Ratchasima, 30000 Thailand*
[b] *School of Physics, Institute of Science, Suranaree University of Technology, Nakhonratchasima, 30000 Thailand*
[c] *Nanotec-Sut Center of Excellence on Advanced Functional Nanomaterials, Suranaree University of Technology, Nakhonratchasima, 30000 Thailand*

Received 9 December 2018; Revised 20 March 2019; Accepted 4 April 2019

Abstract

This work reports the synthesis and electrochemical properties of activated carbon nanofibers composited with lithium manganese silicate (ACNF/Li_2MnSiO_4) for using as an electrode material for energy storage devices. The obtained samples were characterized by means of X-ray diffraction (XRD), scanning electron microscopy (SEM) and Brunauer-Emmett-Teller analyzer (BET). The electrochemical properties were investigated using cyclic voltammetry (CV), galvanostatic charge-discharge (GCD) and electrochemical impedance spectroscopy (EIS). The benefits of ACNF/Li_2MnSiO_4 electrode with maximum surface area and high electrical conductivity leading to an enhance electrochemical performance. The specific capacity of 217.8 F g^{-1} at 0.25 A g^{-1} and 176.4 F g^{-1} at 2 mV s^{-1} is higher than those values of their pure state (ACNF and Li_2MnSiO_4). Moreover, good cycling stability over 90% after 1500 cycles was observed. The interesting electrochemical properties of this composite nanostructure makes it a potential candidate for high performance energy storage devices.

KEYWORDS: Li_2MnSiO_4; Li_2MnSiO_4 composite; Porous carbon composite; Supercapacitors

*Corresponding authors; e-mail: sukanya.ni@rmuti.ac.th

Introduction

With the fast-growing demand for portable electronics market over the past few years, the energy storage devices are required and regarded as the prime power supply. Supercapacitor (SC) is one of the most promising devices for storage energy due to their high power density, and long cycling life [1, 2]. The energy density of this device bridges the gap between conventional capacitors and batteries. According to charge storage mechanism, supercapacitor is classified into two categories of electrical double layer capacitor (EDLC) and pseudo-capacitors. Typically, a pseudo-capacitor (based on metal oxide) exhibits a greater capacitance value than EDLC (based on carbonaceous materials) because their charge storage relies on a pseudo-redox reaction. This is different from EDLCs which store energy by accumulating electrostatic charge at the electrode/electrolyte interface.

Recently, lithium transition metal silicates (Li_2MSiO_4, where M is a transition metal) have been used as electrode materials for energy storage devices due to their high energy density and proper voltage value [3 – 6]. In the crystal structure, the lithium and transition metal cations are situated in tetrahedral sites in a distorted hexagonal close packed oxygen array [7]. Among the Li_2MSiO_4 family, lithium manganese silicate (Li_2MnSiO_4) has been reported as an electrode material both in lithium-ion batteries and supercapacitors [3, 6, 8, 9]. The possible exploration of Mn^{2+}/Mn^{3+} and Mn^{3+}/Mn^{4+} redox chemistry makes Li_2MnSiO_4 achieve high theoretical storage capacitance (~333 mAh g^{-1}) [10]. However, pristine Li_2MnSiO_4 has a low electrical conductivity (around 10^{-14} S cm^{-1}), leading to poor electrochemical performance [11, 12]. To date, numerous approaches have been studied to improve the electrical conductivity of this material [13 – 15]. One of the promising ways is making a composite of Li_2MnSiO_4 with conductive carbon substrates such as activated carbon, CNTs, Graphene [8, 16, 17], in order to decrease the electrolyte ion diffusion distance during charge storage process thus increasing the conductivity. Moreover, several synthetic methods have been used to prepare Li_2MnSiO_4 such as hydrothermal, sol-gel, in situ template method, ball milling [9, 16 – 20].

This work reports the electrochemical performance of ACNF/Li_2MnSiO_4 composite nanostructures synthesized by electrospinning technique followed by heat treatment process. Conceptually, ACNF/Li_2MnSiO_4 composite nanostructures are expected to be advanced electrode materials compared to pure ACNF and Li_2MnSiO_4 due to their combination of high surface area and electrical conductivity of ACNF and electrochemical functionality of Li_2MnSiO_4. In addition, the electrospinning technique was used due to its easy operation and high ability to control the fiber diameter in nanoscale [21].

Materials and Methods

In this work, Polyacrylonitrile (PAN, MW 150,000, Sigma-Aldrich), Dimethylformamide anhydrous (DMF, 99.8%, SIAL), Manganese (II) nitrate hydrate (99.99%, Sigma-Aldrich), lithium acetate dihydrate (99.999%, Sigma-Aldrich), and silicon dioxide nanopowder (Aldrich) were used as the precursor materials. The 1.8 g of PAN powder in 25 ml of DMF solvent was used as the polymer source, whereas lithium acetate, manganese nitrate, and silicon dioxide with the molar ratio of 2: 1: 1 in 5 mL of DMF was used as the metal source. Both precursor sources were mixed and converted into an electrospun by using electrospinning system under an applied voltage of 12 kV, a feeding rate of 0.35 mlh^{-1}, a distance from syringe nozzle to the collector of 12 cm and drum rotating at 800 rpm. The electrospun was stabilized at 250 ºC for 4 h in air atmosphere, carbonized at 750 ºC for 2 h in argon atmosphere to obtain CNF/Li_2MnSiO_4, and activated at 800 ºC for 0.5 h in CO_2 atmosphere to obtain ACNF/Li_2MnSiO_4 composite nanostructure. In this work, two pure states of porous CNF (or ACNF) and Li_2MnSiO_4 are prepared for comparison.

The crystal structure was carried out using X-ray diffraction (XRD, Bruker D2 advance). The morphological was examined by scanning electron microscopy (SEM, Carl Zeiss, Auriga). The surface area was obtained by the Brunauer-Emmett-Teller method (BEL SORP MINI II, JAPAN). The electrochemical properties were tested via cyclic voltammetry (CV), galvanic static charge/discharge (GCD) and electrochemical impedance spectroscopy (EIS) techniques. Three electrodes system of platinum wire, Ag/AgCl and our homemade working electrode was used in 6 M KOH electrolyte. The working electrode was prepared by mixing active material, acetylene black and polyvinylidene difluoride (with a weight ratio of 8:1:1) in NMP solvent and coated on Ni form. The CV measurement was performed between −1.2 and 0 V with the scan rate of 2 – 50 mV s^{-1}. The GCD was operated with the current densities of 0.25 – 10 A g^{-1} while EIS measurements were carried out over a frequency range of 100 kHz to 0.1 Hz.

Results and Discussion

Fig. 1 shows the XRD patterns of ACNF, ACNF/Li_2MnSiO_4, and Li_2MnSiO_4 composite nanostructure after being carbonized at 750 ºC for 2 h. The diffraction peaks of the ACNF/Li_2MnSiO_4 show a significant drop as compared to pure Li_2MnSiO_4 due to the existence of the carbon matrix. The peak at 16.4°, 24.3°, 28.2°, 32.8°, 35.9°, 49.4°, 58.4°, and 59.2° related to crystallite planes of (010), (110), (011), (210), (002), (212), (400), and (230), respectively, of Li_2MnSiO_4 orthorhombic structure with a space group $Pmn2_1$ (PDF card no. 04-015-5273) [22]. The small peak observed at around 17.3° (marked as asterisks) corresponds to (020) crystal plane of impurity Li_2SiO_3 [23]. The diffraction peaks at around 26.0° and 44.0° indicate the formation of graphite structure [24] and can be indexed to (002) and (101) planes of the PDF card no. 75-1621, respectively.

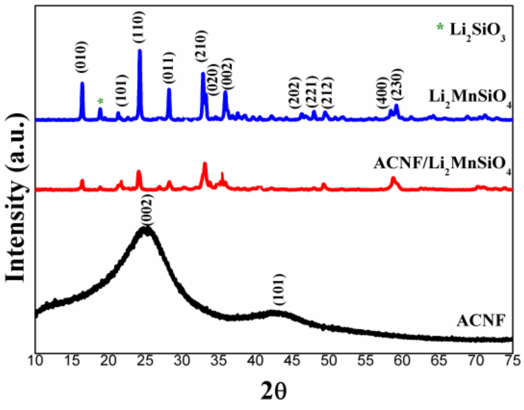

Fig. 1 XRD patterns of ACNF, ACNF/Li_2MnSiO_4, and Li_2MnSiO_4

Fig. 2 shows SEM images of all the prepared samples after they were activated at 800 °C. The ACNF (Fig. 2 (a)) reveals long fiber with shrink surface and uniform in cross-section. For the ACNF/Li_2MnSiO_4 composite nanostructure

(Fig. 2 (b)), the Li_2MnSiO_4 nanoparticles (spherical shape with an average size of 70 nm) are decorated on the ACNF matrix. Moreover, the particles with a variety of shapes and sizes were observed for Li_2MnSiO_4 (Fig. 2 (c)). It is expected that the small diameter of ACNF and particle size of Li_2MnSiO_4 for ACNF/Li_2MnSiO_4 composite nanostructure offer a short length for charge diffusion in the charge storage mechanism

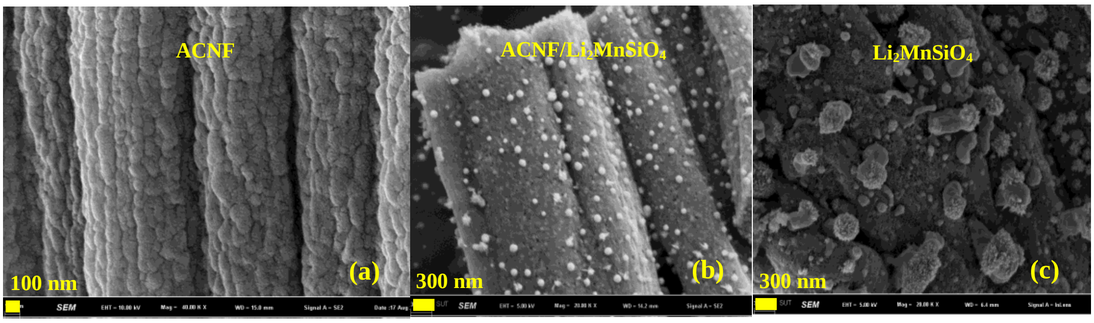

Fig. 2 SEM images of (a) ACNF (b) ACNF/Li_2MnSiO_4, and (c) Li_2MnSiO_4

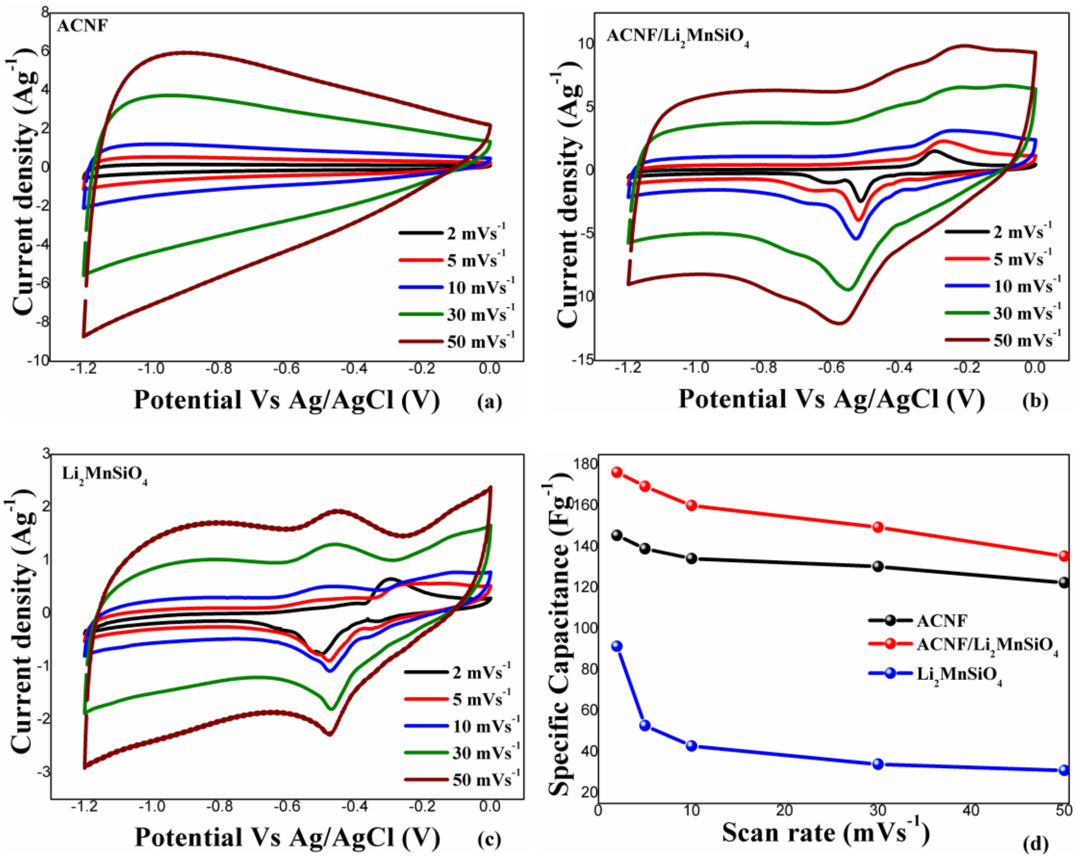

Fig. 3 CV curves at scan rate of 2 – 50 mV s^{-1} for (a) ACNF (b) ACNF/Li_2MnSiO_4 (c) Li_2MnSiO_4 and (d) the corresponding specific capacitance.

Fig. 3 shows CV curves over a wide voltage range of –1.2 – 0 V at a scan rate of 2 – 50 mV s^{-1} for all the prepared samples. The potential windows are very close to the theoretical decomposition voltage of water (1.23 V). Typically, the rounding of CV curve corners are observed in the carbonaceous with resistances electrodes. While the CV curve with redox peak will present in electrode materials that store energy via redox reaction (such as metal oxide). Fig. 3(a) shows CV curves of ACNF at various scan rate. No any redox peaks were observed, confirming the typical EDLC of materials [25]. It is clearly seen that the redox peaks in CV curve of ACNF/Li_2MnSiO_4 (Fig. 3 (b)) and pure Li_2MnSiO_4 electrodes (Fig. 3 (c)), suggesting a charge storage mechanism via the electron transition in Li_2MnSiO_4. According to CV curves, the specific capacitance was calculated as follows

$$C_s = \frac{\int Idv}{mv\Delta V} \tag{1}$$

Where $\int Idv, m, v$ and ΔV are the area under CV curve, active mass, scan rate, and potential window, respectively. The obtained value decreases with an increase in scan rate (Fig. 3 d). The excellent capacitive value was observed for the ACNF/Li_2MnSiO_4 electrode, followed by pure ACNF and Li_2MnSiO_4. The maximum specific capacitance at a scan rate of 2 mV s^{-1} is 176.4, 145.6 and 91.6 F g^{-1}, respectively.

Fig. 4 (a – c) shows the galvanostatic charge/discharge spectra of ACNF, ACNF/Li_2MnSiO_4 and Li_2MnSiO_4, respectively, at 0.25 – 1.0 A g^{-1}. No any voltage drop (IR drop) were observed for all the prepared electrodes. The ACNF/Li_2MnSiO_4 electrode shows longer discharge time than that of ACNF, and Li_2MnSiO_4, respectively (Fig. 4 (d)). According to the spectra, the specific capacitance values (C_s) are calculated from the discharge time according to equation (2);

$$C_s = \frac{I\Delta t}{m\Delta V} \tag{2}$$

Where $I, \Delta t, m$ and ΔV are the applied current, discharging time, active mass and the potential window, respectively. The corresponding energy density (E) and power density (P) are calculated using equation (3 – 4)

$$E = \frac{1}{2} C_s \left(\Delta V\right)^2 \tag{3}$$

$$P = \frac{E}{\Delta t} \times 3600 \tag{4}$$

The obtained specific capacitance for ACNF, ACNF/Li_2MnSiO_4, and Li_2MnSiO_4 electrodes are shown in Fig. 5 (a). By varying the current densities (0.25 – 10.0 A g^{-1}), the specific capacitance decreases with an increase in current density. Such behavior may be due to activation and concentration polarizations at high current densities which results in low utilization of the active materials [6]. The maximum values at 0.25 A g^{-1} are listed in Table. 1. Moreover, the corresponding Ragone plot is presented in Fig. 5 (b).

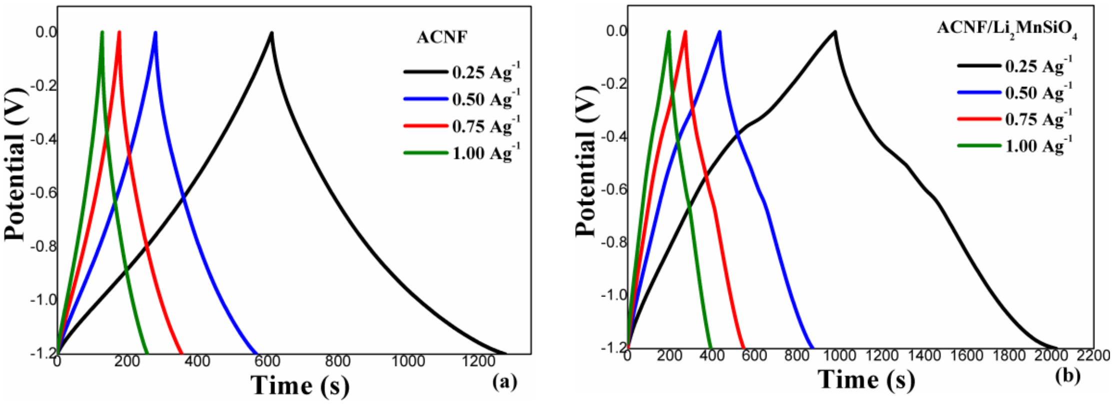

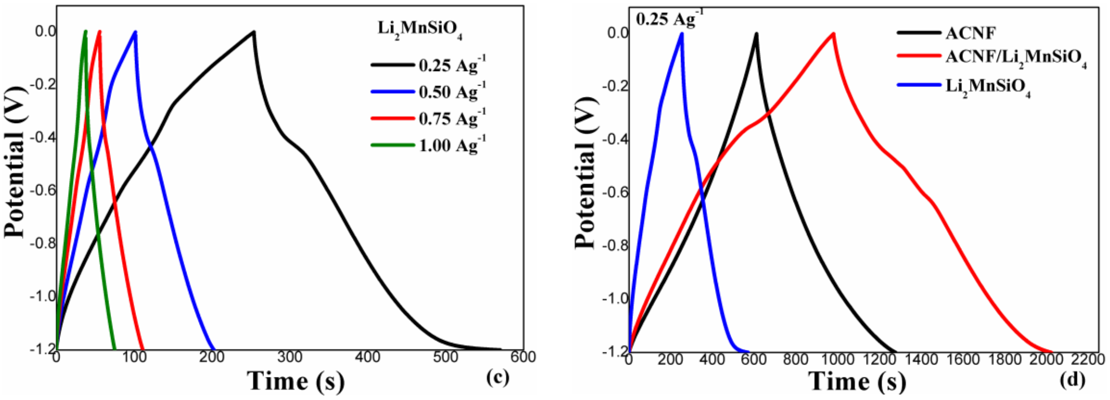

Fig. 4 Galvanostatic charge/discharge spectra at 0.25 – 1.0 A g^{-1} for (a) ACNF (b) ACNF/Li_2MnSiO_4 and (c) Li_2MnSiO_4, and (d) The comparison spectra at 0.25 A g^{-1} for all prepared sample.

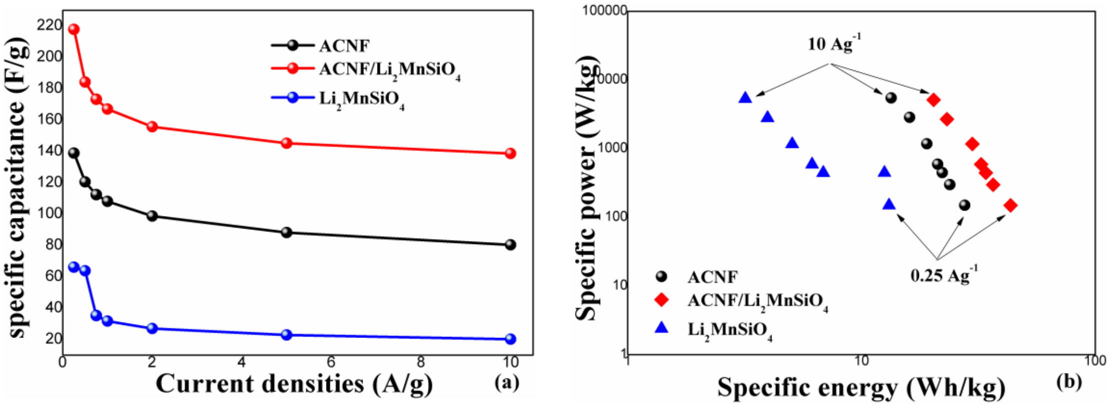

Fig. 5 (a) The discharge specific capacitance and (b) the corresponding Ragone plot for ACNF, ACNF/Li_2MnSiO_4 and Li_2MnSiO_4 electrodes.

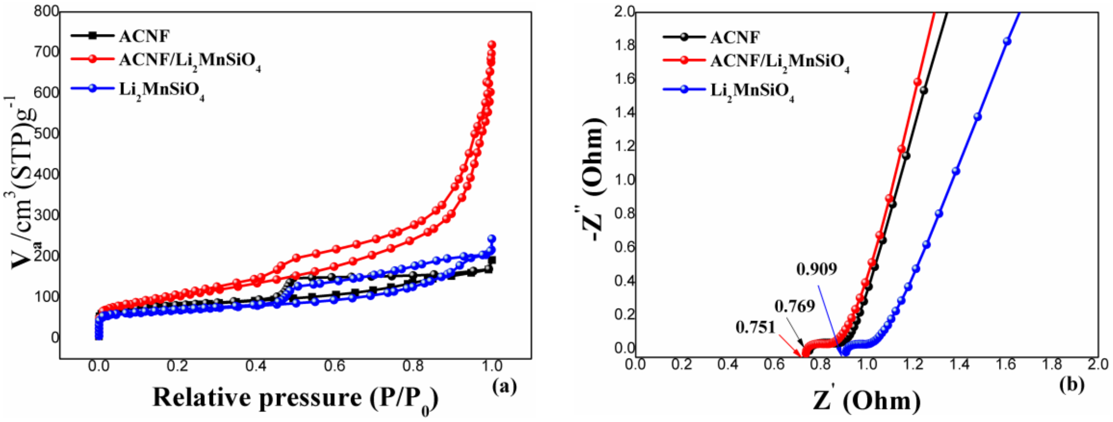

Fig. 6 Adsorption-desorption isotherms (a) and Nyquist plots (b) for ACNF, ACNF/Li_2MnSiO_4 and Li_2MnSiO_4 electrodes

The excellent capacitive behavior of the ACNF/Li_2MnSiO_4 electrode can be attributed to the high surface area and electrical conductivity of materials. Fig. 6 (a) shows the adsorption and desorption isotherms for all the prepared samples. The isotherms exhibit IUPAC type IV pattern, indicating the existence of mesoporous. The specific surface area of 219, 351, and 197 $m^2\ g^{-1}$ was observed for ACNF, ACNF/Li_2MnSiO_4 and, Li_2MSiO_4, respectively. The large surface area of ACNF/Li_2MnSiO_4 increased the effective contact area between electrode and electrolyte, supporting a large number of reaction sites, resulting in an improved specific capacitance. Fig. 6 (b) shows the Nyquist plots for all prepared electrodes. The plots of all materials show a semicircle in high-frequency region related to the charge-transfer resistance (R_{ct}). The larger the diameter of the semi-circle, the higher the charge-transfer resistance [26]. The intercept at x-axis refers to the series resistance (R_s). The values of 0.769, 0.751, 0.909 Ω were observed for ACNF, ACNF/Li_2MnSiO_4 and Li_2MnSiO_4, respectively. The lowest R_s value for ACNF/Li_2MnSiO_4 signifies the highest current density thus the highest conductivity.

Fig. 7 shows the plot of the specific capacitance after repeated CV at a scan rate of 50 mV s^{-1} over 1500 cycles. The best stability of ACNF electrode may be due to the network carbon matrix which restricts the change of electrode volume during the charge/discharge process. The fastest specific capacity fading was observed in Li_2MnSiO_4 electrodes. Such behavior is mainly attributed to redox reaction arising from Li_2MnSiO_4 nanoparticle which causes damage to the structure during charge/discharge process, and thus leading to poor cycling stability. The ACNF/Li_2MnSiO_4 electrode shows about 93% remaining after 1500 cycles indicating long term cycling stability possibly due to free space between the Li_2MnSiO_4 nanoparticles with ACNF matrix working as an elastic buffer.

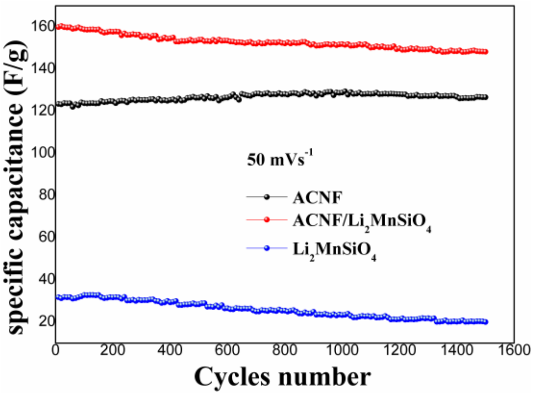

Fig. 7 the specific capacitance after 1500 cycles at a scan rate of 50 mV s^{-1}

Table 1 Shows lists of surface area, mean pore diameter, series resistance, specific capacitance, energy density, and power density.

Samples	Surface area ($m^2\ g^{-1}$)	Mean pore diameter (nm)	series resistance (Ohm)	CV (2 mV s^{-1})	GCD (0.25 A g^{-1})		
				C_s (F g^{-1})	C_s (F g^{-1})	E (Wh kg^{-1})	P (W kg^{-1})
ACNF	219	4.76	0.769	145.6	138.9	27.67	149.72
ACNF/Li_2MnSiO_4	351	9.84	0.751	176.4	217.8	43.40	149.74
Li_2MnSiO_4	197	6.55	0.909	91.6	66.2	13.212	149.37

Conclusion

In summary, ACNF/Li_2MnSiO_4 composite nanostructures were synthesized by electrospinning followed by carbonization and activation process. By making a composite nanostructure of ACNF and Li_2MnSiO_4, the surface area, electrical conductivity, the specific capacity, and the stability improved compared to their pure states. The stability over 90% was observed after 1500 cycles. The maximum specific capacitance value of 176.4 F g^{-1} at 2 mV s^{-1} (using CV scan) and 217.8 F g^{-1} at 0.25 A g^{-1} (using GCD) are achieved. The superior capacitance could be explained by (i) the fibrous with optimized pore supported high surface area for electrolyte ions penetration, resulting in an improved EDLC (ii) lower equivalent series resistances giving rise to higher conductivity and (iii) the Faradaic reactions of Li_2MnSiO_4 nanoparticles supported pseudo-capacitance. These results demonstrate that using the ACNF/Li_2MnSiO_4 composites nanostructure as an electrode material for energy storage devices could be ideal.

Acknowledgements

This work is supported by Rajamangala University of Technology Isan. Contract No. NKR2561REVO35. The authors are thankful to the department of Applied Physics Rajamagala University of Technology Isan (RMUTI), the Advanced Material Physics Laboratory (AMP) at Suranaree University of Technology (SUT), and the Center for Scientificand Technological Equipment, Suranaree University of Techanolgy, for all facilities.

References

[1] Y.Q. Zhao, M. Lu, P.Y. Tao, Y.J. Zhang, X.T. Gong, Z. Yang, G.Q. Zhang, H.L. Li, Hierarchically porous and heteroatom doped carbon derived from tobaccorods for supercapacitors, J. Power Sources. 307 (2016) 391 – 400.

[2] X. Cui, R. Lv, R.U.R. Sagar, C. Liu, Z. Zhang, Reduced graphene oxide/carbon nanotube hybrid film as high performance negative electrode for supercapacitor, Electrochim. Acta. 169 (2015) 342 – 350.

[3] A. Nyten, A. Abouimrane, M. Armand, T. Gustafsson, J.O. Thomas, Electrochemical performance of Li_2FeSiO_4 as a new Li-battery cathode material, Electrochem. Commun. 7 (2005) 156 – 160.

[4] R. Dominko, M. Bele, M. Gaberscek, A. Meden, M. Remskar, J. Jamnik, Structure and electrochemical performance of Li_2MnSiO_4 and Li_2FeSiO_4 as potential Li-battery cathode materials, Electrochem. Commun. 8 (2006) 217 – 222.

[5] C. Lyness, B. Delobel, A.R. Armstrong, P.G. Bruce, The lithium intercalation compound Li_2CoSiO_4 and its behavior as a positive electrode for lithium batteries, Chem. Commun. 46 (2007) 4890 – 4892.

[6] K. Karthikeyan, V. Aravindan, S.B. Lee, I.C. Jang, H.H. Lim, G.J. Park, M. Yoshio, and Y.S. Lee, Electrochemical performance of carbon-coated Li_2MnSiO_4/Activated carbon for an asymmetric hybrid supercapacitor, J. Power Sources. 195 (2010) 3761 – 3764.

[7] R.J. Gummow and Y. He, Recent progress in the development of Li_2MnSiO_4 cathode materials, J. Power Sources. 253 (2014) 315 – 331.

[8] P. Chaturvedi, A. Sil., Y. Sharma, Energy storage performance of hybrid aqueous supercapacitor based on nano-Li_2MnSiO_4 and activated carbon, Ionics 22 (2016) 1719 – 1728.

[9] S. Qiu, X. Pu, X. Ai, H. Yang, Z. Chen, Y. Cao, Template synthesis of mesoporous Li_2MnSiO_4@C composite with improved lithium storage properties, Electrochim. Acta. 291 (2018) 124 – 131.

[10] V. Aravindan, K. Karthikeyan, K.S. Kang, W.S. Yoon, W.S. Kim, Y.S. Lee, Influence of carbon towards improved lithium storage properties of Li_2MnSiO_4 cathodes, J. Mater. Chem. 21 (2011) 2470.

[11] R. Dominko, Li_2MnSiO_4 (M=Fe and/or Mn) cathode materials, J. Power Sources. 184 (2008) 462 – 468

[12] V. Ramar, P. Balaya, The effect of polymorphism on the lithium storage performance of Li_2MnSiO_4, J. Power Sources. 306 (2016) 552 – 558

[13] S. Liu, J. Xu, D. Li, Y. Hu, X. Liu, K. Xie, High capacity Li_2MnSiO_4/C nanocomposite prepared by solegel method for lithium-ion batteries, J. Power Sources. 232 (2013) 258 – 263.

[14] P. Zhai, S. Zhao, H. Cheng, J. Zhao, C. Nan, Synthesis and structural stability of $Li_{2.1}Mn_{0.9}[PO_4]_{0.1}[SiO_4]_{0.9}$/C mixed polyanion cathode material for Li-ion battery, Electrochim. Acta. 153 (2015) 217 – 224.

[15] Y. Pei, Q. Chen, C. Xu, H. Wang, H. Fang, C. Zhou, L. Zhen, G. Cao, Chelateinduced formation of Li_2MnSiO_4 nanorods as a high capacity cathode material for Li-ion batteries, J. Mater. Chem. 4 (2016) 9447 – 9454.

[16] T. Peng, W. Guo, Q. Zhang, Y. Zhang, M. Chen, Y. Wang, H. Yan, Y. Lu, Y. Luo, Uniform coaxial CNT@Li_2MnSiO_4@C as advanced cathode material for lithium ion battery, Electrochim. Acta. 291 (2018) 1 – 8.

[17] H. Zhu, H. He, X. Xin, X. Ma, L. Zan, Y. Zhang, Facile synthesis of Li_2MnSiO_4/C/graphene composite with superior high-rate performances as cathode materials for Li-ion batteries, Electrochim. Acta. 155 (2015) 116 – 124.

[18] S. Devaraj, M. Kuezma, C.T. Ng, P. Balaya, Sol-gel derived nanostructured Li_2MnSiO_4/C cathode with high storage capacity, Electrochimica Acta. 102 (2013) 290 – 298.

[19] X. Wu, S.X. Zhao, L. Wei, H. Deng, C.W. Nan, Improving the structure stability and electrochemical performance of Li_2MnSiO_4/C cathode materials by Ti-doping and porous microstructure, J. Alloy. Comp. 735 (2018) 1158 – 1166.

[20] B. Shao, I. Taniguchi, Synthesis of Li_2MnSiO_4/C nanocomposites for lithium battery cathode employing sucrose as carbon source, Electrochim. Acta. 128 (2014) 156 – 162.

[21] S.Y. Gu, O.L. Wu, J. Ren, Preparation and surface structures of carbon nanofibers produced from electrospun PAN precursors, New Carbon Mater. 23(2) (2008) 171.

[22] Y. Wang, Y. Xia, A new concept hybrid electrochemical supercapacitor: carbon/$LiMn_2O_4$ aqueous system, Electrochem. Commun. 7 (2005) 1138 – 1142.

[23] P.V. Subha, Balagonpal N. Nair, P. Hareesh, A. Peer Mohamed, T. Yamaguchi, K.G.K. Warrier and U.S. Hareesh, Enhanced CO_2 absorption kinetics in lithium silicate platelets synthesized by a sol-gel approach, J. Mater. Chem. A. 2 (2014) 12792.

[24] W. Wang, P. Liu, M. Zhang, J. Hu, F. Xing, The pore structure of phosphoaluminate cement, Open J. Compos. Mater. 2 (2012) 104 – 112.

[25] Z.B. Wen, Q.T. Qu, Q. Gau, Z.H. Hu, Y.P. Wu, X.W. Zheng, Y.F. Liu, X.J. Wang, An activated carbon with high capacitance from carbonization of a resorcinol-formaldehyde resin, Electrochem. Commun. 11 (2009) 715 – 718.

[26] A.K. Das, S.K. Karan, B.B. Khatua, High energy density ternary composite electrode material based on polyaniline (PANI), molybdenum trioxide (MoO_3) and graphene nanoplatelets (GNP) prepared by sonochemical method and their synergistic contributions in superior supercapacitive performance, Electrochim. Acta. 180 (2015) 1 – 15.